Journal of Energy Storage 75 (2024) 109694

Contents lists available at ScienceDirect

Journal of Energy Storage

journal homepage: www.elsevier.com/locate/est

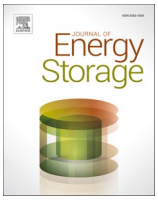

Research Papers

PEM Electrolyzer Digital Replica based on internal resistance determination applied to hydrogen energy storage

Francisco Javier Folgado *, Isaías González, Antonio José Calderón

Department of Electrical Engineering, Electronics and Automation, Universidad de Extremadura, Avenida de Elvas, s/n, Badajoz 06006, Spain

ARTICLE INFO

Keywords:
PEM Electrolyzer
Hydrogen
Microgrid
Digital Replica
Model
Energy storage

ABSTRACT

The rise of hydrogen as an energy storage means and its associated technologies have prompted the implementation of hydrogen generation systems based on electrolyzers. Electrolyzers exhibit complex behaviour and their implementation is not immediate, leading to the use of tools such as Digital Replicas (DR) for their study. This paper presents a DR for a Proton Exchange Membrane Electrolyzer (PEMEL) through the development of an Equivalent Circuit Model (ECM) that describes the static behaviour of the individual cells comprising it. This research is focused on contributing to hydrogen generation with the main objective of using this energy vector for energy storage applications. For this purpose, an installation consisting of a PEMEL and a set of auxiliary equipment required for its proper operation and for measuring key electrolyzer parameters such as current, voltage, hydrogen flow rate, temperature, etc. is implemented. Furthermore, a Data Acquisition System (DAQ) is available to collect process information for later analysis. The PEM cell model is obtained through an experimental process based on the determination of internal resistance to calculate the remaining key parameters. The successful functioning and suitability of the DR and developed model are reported through experimental data obtained from the PEMEL under operating conditions.

1. Introduction

The escalating energy demand and the scarcity of traditional resources like fossil fuels have driven the advancement and exploration of renewable energy technologies. Among these, solar thermal and photovoltaic technologies are extensively investigated and deployed for various industrial and domestic purposes. These technologies are continuously researched to enhance their performance via energy management approaches [1] and novel materials [2,3]. Additionally, modern technologies and processes have been developed to harness emerging renewable energy sources such as hydrogen. The importance of this element has been increasing in recent years, making its presence felt through applications in multiple sectors such as the automotive industry [4], healthcare [5], and energy [6].

Hydrogen generation is carried out through devices called electrolyzers. These devices allow the separation of a compound into its primary parts through the electrochemical process of electrolysis. Electrolyzers fall into four categories: alkaline, Proton Exchange Membrane (PEM), solid oxide, and Anion Exchange Membrane (AEM). The main difference between these types is the nature of the electrolyte that enables electrolysis. Alkaline types employ liquid electrolyte solutions like potassium hydrogen (KOH) or sodium hydroxide (NaOH) [7]. PEM types incorporate solid polymer membranes as electrolytes [7,8]. Solid oxide types utilize solid ceramic electrolytes [9]. Lastly, AEM electrolyzers generate hydrogen from a semi-permeable membrane that allows the passage of hydroxide ions (OH-) [7,10]. The hydrogen produced by such equipment is commonly denoted by colour, which varies based on the input compound and the energy source used. Thus, hydrogen generated from water and renewable energy sources is recognized as green hydrogen [11]. Fuel cells, serving as counterparts to electrolyzers, operate in reverse, producing electricity by consuming hydrogen [12]. Another application for hydrogen is energy storage. Nowadays, various physical and chemical methods are employed, including compression, liquefaction processes, and solid-state techniques such as metal hydrides [13]. The application of these storage methods, tailored to specific characteristics and diverse storage capacities, demonstrates the potential for advancing the future hydrogen-based economy [14,15].

In the energy sector, the availability of hydrogen as an alternative energy source, achieved through the combination of electrolyzers and fuel cells, has induced a transformation in prevailing paradigms within

* Corresponding author.
E-mail addresses: ffolgar@unex.es (F.J. Folgado), igonzp@unex.es (I. González), ajcalde@unex.es (A.J. Calderón).

https://doi.org/10.1016/j.est.2023.109694
Received 23 May 2023; Received in revised form 6 October 2023; Accepted 9 November 2023
Available online 18 November 2023
2352-152X/© 2023 The Author(s). Published by Elsevier Ltd. This is an open access article under the CC BY license (http://creativecommons.org/licenses/by/4.0/).

systems such as microgrids and smart microgrids. Microgrids consist of a cluster of loads, distributed generation units and energy storage systems operated in coordination to reliably supply electricity, connected to the host power system at the distribution level [16,17]. The smart connotation refers to the system's capacity for self-management through dedicated elements, such as Programmable Logic Controllers (PLC) [18]. These adaptable systems facilitate the incorporation of new hydrogen-harnessing devices, resulting in hybrid systems that blend renewable energies with hydrogen technology [6]. In this context, PEM electrolyzers (PEMEL) are employed alongside water for hydrogen generation. The use of hydrogen as an energy storage solution, supplying microgrids during periods of generation shortfall or heightened energy demand, is emphasized [19]. This approach mitigates energy fluctuations within the microgrid over the medium to long term [20]. Notably, PEMEL are favoured in renewable energy applications due to their swift response to fluctuations in input conditions [21]. Moreover, the significance of hydrogen and electrolyzers is highlighted as a strategic approach aligned with the UN Sustainable Development Goals. Specifically, hydrogen is anticipated to contribute to the fulfilment of Goal 7, promoting accessible and clean energy [22].

Concerning their operation, the intricate nature of electrolyzers poses challenges to their direct integration into a process or system. Thus, a thorough analysis of the device is essential to comprehend its behaviour and interaction with other system components. Digital Replicas (DR) play a crucial role in this study. A DR can be described as a virtual version of the physical device, replicating its real-time operation. Nonetheless, there is currently no single generally accepted definition for the concept of DR. Therefore, in the framework of this research, the definition given in [23] has been considered, which defines DR as the interaction between two parts: the model of the physical system and the connection/communication for data exchange between model and real system. This model can take different forms, such as those based on equations or physical laws [24] or black-box models, like neural networks [25]. For PEMEL, the most commonly used models are Equivalent Circuit Models (ECM), whose electrical components are related to the physical effects of the device's operation [26]. This digital tool streamlines device study without requiring physical disposal, isolating it from other components. DR facilitates testing various conditions, including those beyond real system limits due to technical or economic factors [27].

To undertake this research, a brief literature review has been conducted, focusing on works related to: diverse models of PEMEL, applications of these devices in the energy sector, and papers detailing the equipment and methodology employed. In Atlam and Kolhe [20], the behaviour of a PEM cell is described using an ECM model. In this work, the various key parameters of the cell as well as the effect of working temperature and pressure on these parameters are studied. In addition, an expression is introduced for the voltage of a PEMEL as a function of the number and distribution of the cells that compose it. Awasthi et al. [24] develop a model for a PEM cell under elevated temperature and pressure operating conditions using MATLAB-Simulink. This model is used to determine the cell voltage and perform a graphical comparison of the results. In Ismail et al. [28], a photovoltaic system for hydrogen production is modelled and simulated, where the PEMEL model is developed using experimental data to obtain the voltage-current relationship and determine the optimal operating point of the system. Analogously, Albarghot et al. [29] describe a model for a solar panel - PEMEL system at laboratory scale, where the hydrogen flow rate produced is studied employing a MATLAB-Simulink simulation of the model. In Guilbert and Vitale [30], the modelling of a PEMEL using a dynamic behaviour analysis is reported. In this analysis, the key parameters of the PEMEL are studied and the experimental process followed for their determination is explained. In Espinosa-López et al. [31], the modelling and validation of a 46 kW PEMEL operating at high pressure are carried out, where the effect of the working temperature on the behaviour of the electrolyzer is studied. The model is designed in MATLAB-Simulink and the results obtained are validated graphically and employing statistical metrics. The model described in Hernández-Gómez et al. [32] studies the static-dynamic behaviour of the cell voltage for a PEMEL under adaptive parameters.

The literature reviewed reinforces the presence of a wide variety of models, describing the behaviour of the PEMEL under a multitude of operating conditions for applications in the energy sector. Nonetheless, scarce details have been found regarding the description of the physical equipment used for the development of the model, as well as the experimental process executed for its determination. Additionally, there is a noticeable trend to validate models based on voltage-current comparisons, sometimes overlooking important PEMEL parameters such as power consumption and hydrogen flow rate. Graphical comparative curves are frequently used to present these results, occasionally with statistical analysis.

The work presented in this paper is motivated by the research gaps identified in the reviewed literature. As a result, this study covers the three key topics sought in the literature, with a special focus on detailing the equipment employed and outlining the experimental process conducted.

This paper describes the design and validation of the DR of a PEMEL employing an ECM-based model. This model focuses on reproducing the static operation of the individual cells that compose the PEMEL. For this purpose, an installation has been set up with equipment dedicated to the correct operation of the PEMEL and its study for the determination of the model. Furthermore, the experimental process performed to develop the cell model is described, which aims to determine the cell voltage using the calculation of the internal resistance. The DR generated from the PEMEL is studied under nominal operating conditions, analysing the results obtained at the individual cell level and as a stack.

The aforementioned PEMEL and its ancillary equipment comprise the hydrogen generation subsystem, whose operation is framed within a photovoltaic-powered smart microgrid hybridized with green hydrogen. This generation subsystem aims to produce green hydrogen for energy storage purposes, intended for subsequent application through a fuel cell. Previous works describe the set of equipment that constitutes the smart microgrid, as well as its operation [33,34].

The structure of the rest of the manuscript is as follows. Section 2 describes the principle of operation of the electrolyzer, as well as the implemented setup and equipment associated with the operation of the PEMEL. Section 3 details the design of the model and the experimental process conducted to obtain it. Section 4 illustrates the results obtained from the deployment of the DR and a discussion thereof. Finally, the most relevant conclusions of the study are presented.

2. Materials and methods

2.1. Fundamentals of electrolysis in PEMEL

As mentioned above, the electrolyzer is a device that generates hydrogen from a compound through the process of electrolysis. These devices are composed of a set of cells that are responsible for carrying out electrolysis. These cells can be arranged in series, referred to as a stack, or in parallel. In the case of a water-fed PEMEL, the cell structure is illustrated in Fig. 1.

Within the cell, electrolysis is performed as a result of two processes: a reduction at the cathode and an oxidation at the anode. Both processes are defined in Eq. (1) and Eq. (2) respectively.

$$2H^+ + 2e^- \rightarrow H_2 \tag{1}$$

$$H_2O \rightarrow 2H^+ + \frac{1}{2}O_2 + 2e^- \tag{2}$$

The electrolysis process resulting from both half-reactions is indicated in Eq. (3):

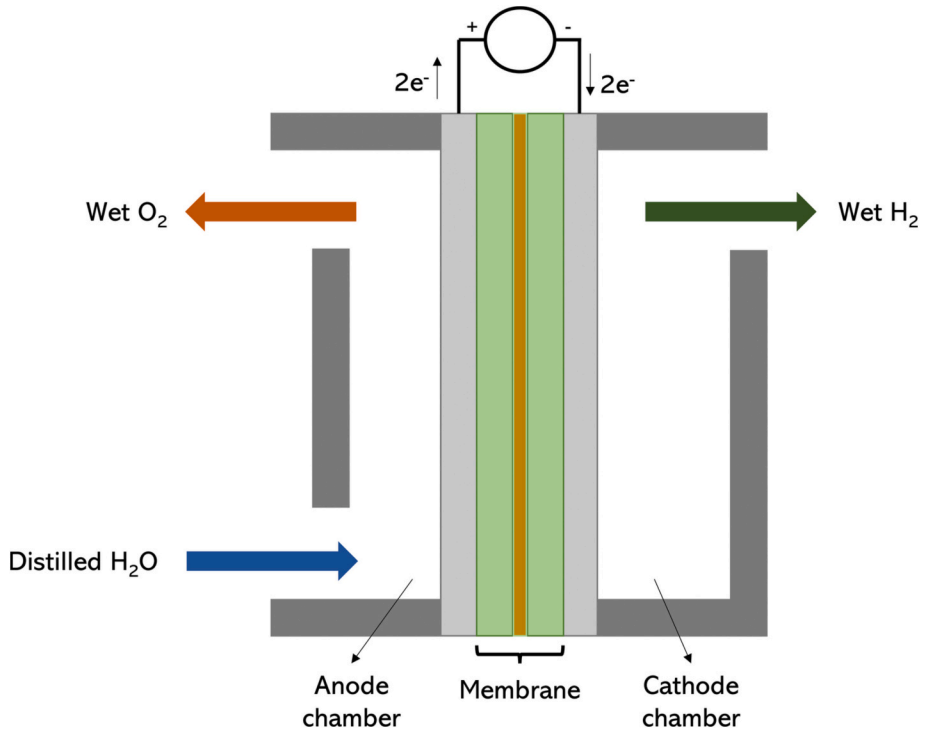

Fig. 1. Structure and operation of a PEM cell.

$$H_2O \rightarrow H_2 + \frac{1}{2}O_2 \quad (3)$$

2.2. PEM Electrolyzer and ancillary equipment

For this research, a 6-cell stack PEMEL has been employed. The geometry and number of cells of the stack are depicted in Fig. 2a. In Fig. 2b, the installed stack is displayed, where several components are coupled to it: a PT-100 temperature sensor [35] is located on the lateral part to monitor the operating temperature of the stack. A fan [36] is installed on the frontal part to control the working temperature within the nominal operating range of the PEMEL. Finally, a connector has been included on the bottom of the stack to collect the voltages of each cell, which is a crucial aspect for the development of the model that is further explained below.

Table 1 lists the main technical specifications for the operation of the electrolyzer.

Table 1
Technical specifications of the electrolyzer.

Number of cells	6 cells in series
Input current (A)	0 to 8 A
Stack voltage (V)	12 to 15 V
Working pressure (bar)	0.1 to 6 bar
Working temperature (°C)	25 to 50 °C
Flow rate generated (ml/min)	250 ml/min; 15 Nl/h
Hydrogen purity	>99.9999 %
Dimensions (mm)	267 × 382 × 470 mm

The electrolysis process described in Section 2.1 results in wet hydrogen, i.e. hydrogen with water content. This is due to the non-ideality of the electrolyzer, which results in the need to employ additional equipment for the removal of this unwanted moisture to obtain high-purity dry hydrogen. To this end, a series of auxiliary equipment complementary to the electrolyzer has been installed to achieve dry

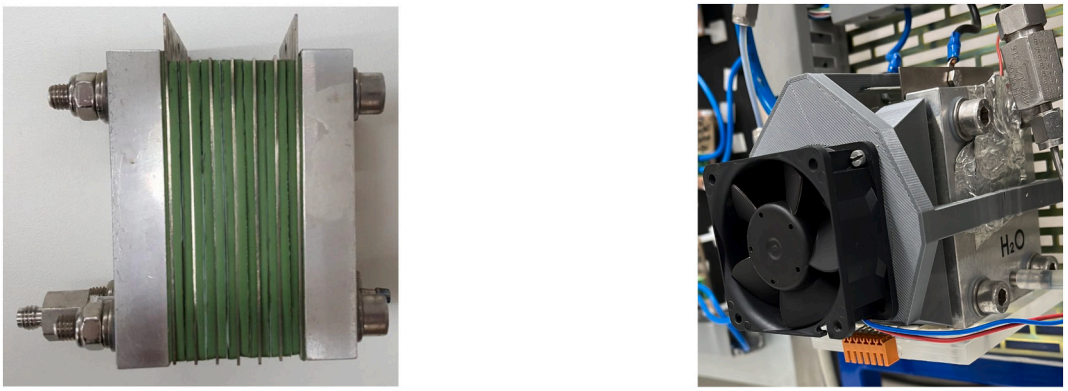

Fig. 2. PEM Electrolyzer. (a) Stack appearance and number of cells. (b) Stack installed alongside coupled elements.

hydrogen. The installation and each of the components are detailed below.

First, the electrical current is supplied to the hydrogen generation subsystem via a low voltage DC bus, materialised by a Lithium-Ion battery (referred to as 'Microgrid power supply' in Fig. 3). This DC bus ensures a reference voltage level as well as a smooth and stable power flow to the PEMEL. This flow from the DC bus is directed to the input of the PEMEL through a programmable DC/DC converter [37]. The programmable feature of the converter enables to adjust its output in order to suit the desired working point of the PEM stack.

The water flow is supplied by gravity from a tank above the stack. After the electrolysis process, the resulting oxygen is returned to the water tank, while the wet hydrogen is transferred to a phase separator. Within the phase separator, the water particles descend by gravity and accumulate at the bottom part, where they are redirected to the water tank for re-utilisation. Meanwhile, the hydrogen flows through a series of silica filters that remove the remaining humidity from the hydrogen to produce a dry, high-purity product. Finally, the dry hydrogen flow rate is measured utilising a flow meter [38] and stored in a metal hydride bottle. Moreover, the pressure of the hydrogen circuit is obtained using a pressure sensor [39]. Fig. 3 depicts the described installation employing a diagram based on synoptics, detailing the location of each device and the flow of products and sub-products resulting from its operation. In addition, Fig. 4 shows the appearance of the installation, where the components involved can be observed. In addition, the PLC employed for data acquisition is displayed in the bottom right-hand margin.

2.3. Data acquisition system

To develop the model discussed in this research, a data acquisition system (DAQ) was employed to capture essential electrolyzer performance parameters during experimentation.

Sensors and actuators controlling the PEMEL process were connected to a Siemens S7–1500 PLC [40]. This facilitated real-time data collection of key PEMEL variables. For process visualisation and data storage, a user-friendly Graphical User Interface (GUI) has been developed in LABVIEW [41]. LABVIEW software is oriented to the design and implementation of a diversity of systems, highlighting GUIs and SCADA systems, through a graphical programming language and a wide variety of tools and synoptics [33].

Regarding the operation of the DAQ, the data acquired by the PLC is read by the GUI through a client-server structure based on the Open Platform Communications (OPC) protocol. OPC is a widely used standardised data exchange technology to deal with heterogeneity and interoperability in automation systems. [42].

The GUI developed acts as the OPC client, simultaneously performing the functions of visualisation and data storage. The visualisation of the process information is achieved using graphs and numerical indicators that display the real-time status of the key variables of the PEMEL. On the other hand, data storage is accomplished by exporting the read data to an Excel spreadsheet. This storage is crucial for the disposal the acquired data in a more manageable format to facilitate subsequent processing. Fig. 5 depicts the DAQ elements, information flow, and communication among them.

3. Model development

3.1. Cell Equivalent Circuit Model

The ECM is a tool that allows representing the operation of a device through an electrical schematic composed of simple components such as power sources, resistances, capacitors, coils, etc. Particularly for PEMEL, and as indicated in Section 1, there is a wide variety of models in the literature reviewed. These models are mainly distinguished by their application context and complexity. Simplified models describe the behaviour of the PEMEL using an electrical diagram with few components, addressing the study of its operation in a more general manner. In contrast, more complex models are highlighted by more detailed electrical diagrams, where a more thorough study is conducted, and specific phenomena/effects are related to certain electrical components.

For this research, a simplified model of the PEMEL cell is proposed to describe its static behaviour, employing two components: a power supply and a resistance. These elements are used in other well-known models such as those of Atlam and Kolhe [20] and Guilbert and Vitale [30] to describe the electrolysis process and the energy losses incurred, respectively. Moreover, these components rely on parameters like

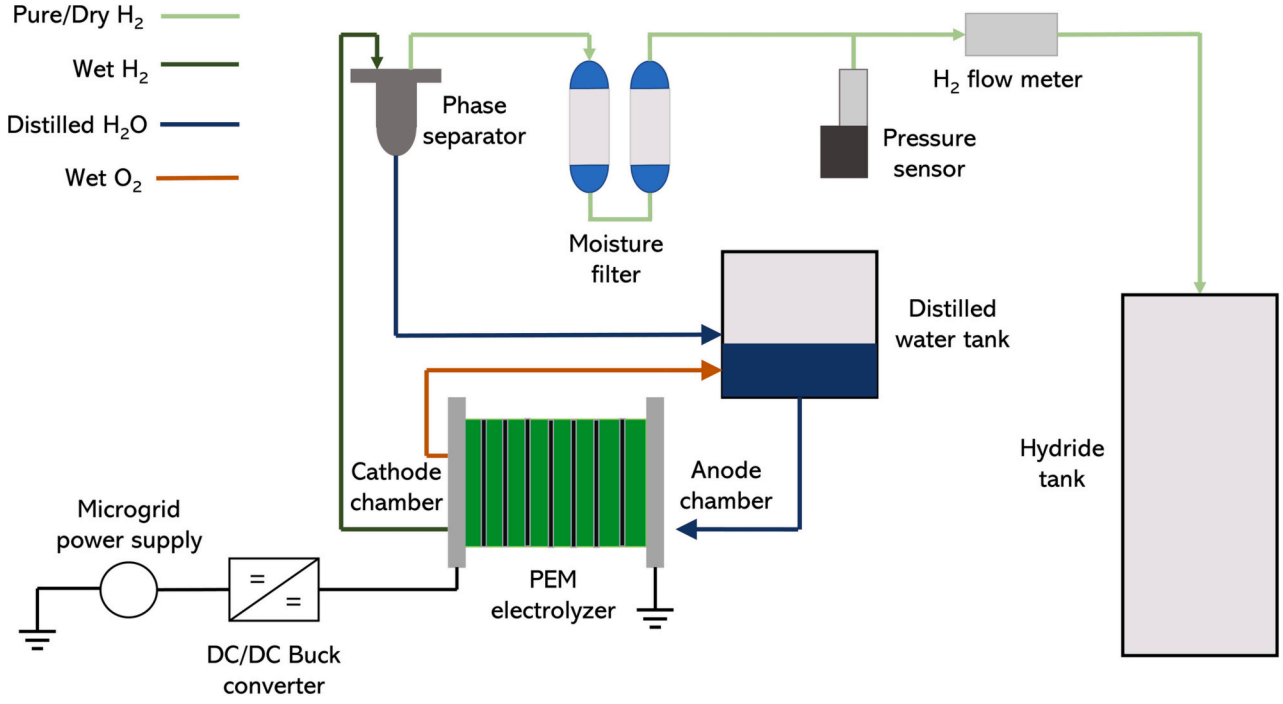

Fig. 3. PEMEL and complementary equipment for high-purity dry hydrogen generation and storage.

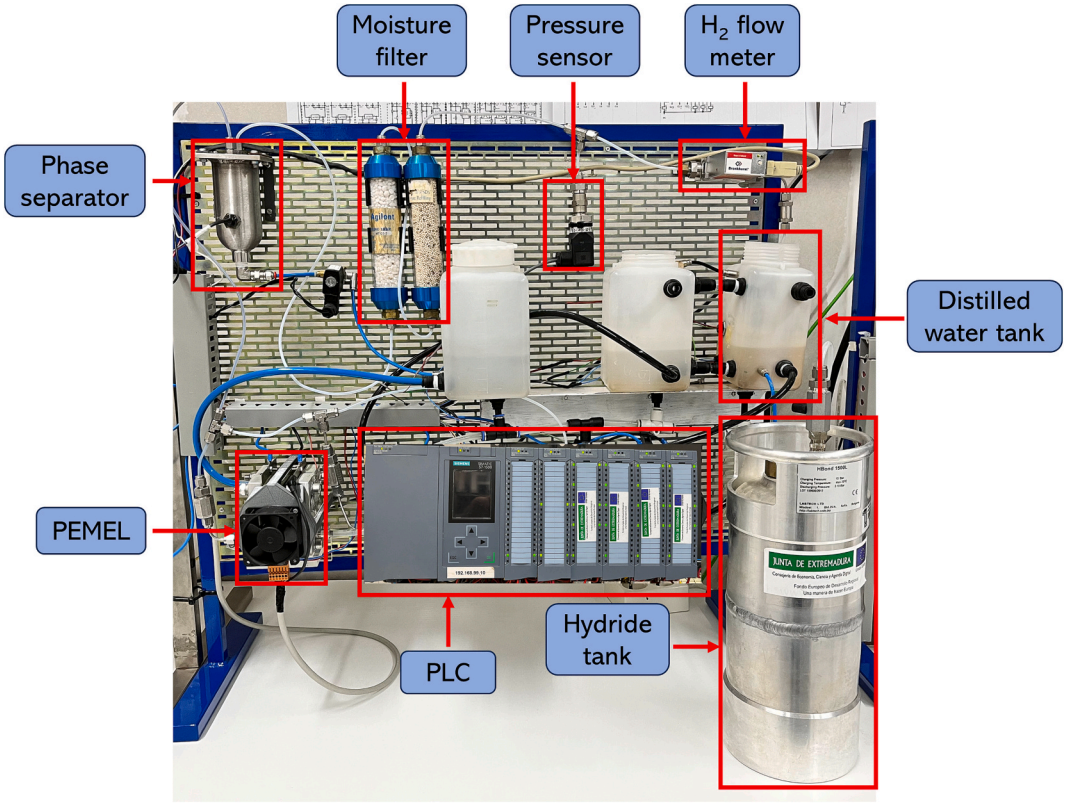

Fig. 4. Installation appearance and equipment employed.

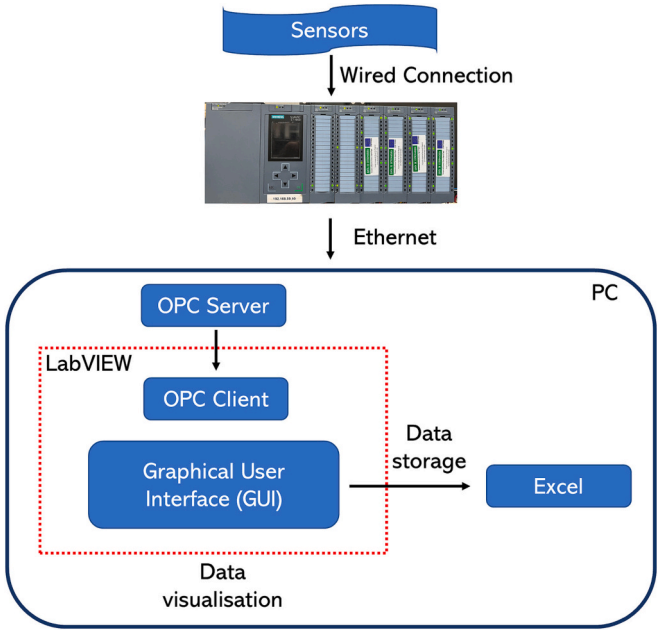

Fig. 5. DAQ for visualisation and storage of process data.

temperature, pressure, and input current. This allows for studying the effects of fluctuation on cell operation. Fig. 6 depicts the ECM utilised in the PEM cell.

Where I (A) refers to the current consumed, R_{int} (Ω) is the internal resistance that simulates the power dissipation due to cell operation, and V_{int} (V) is the ideal (electrochemical) voltage or potential required for the electrolysis process. Thus, the cell voltage V_{cell} (V) is defined in Eq. (4) as:

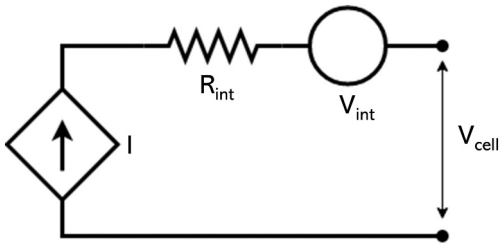

Fig. 6. ECM of the PEM cell.

$$V_{cell} = IR_{int} + V_{int} \tag{4}$$

V_{int} is calculated in Eq. (5) based on the Gibbs free energy ΔG (J mol^{-1}) and Faraday's constant (96,487 C mol^{-1}) [43]:

$$V_{int} = \frac{\Delta G}{2F} \tag{5}$$

For liquid water, ΔG is obtained by Eq. (6) for a given temperature T (°C) [43]:

$$\Delta G = 285840 - 163.2(273 + T) \tag{6}$$

The power consumed in the electrolysis process $P_{e,cell}$ (W) is obtained from the ideal voltage employing Eq. (7):

$$P_{e,cell} = IV_{int} \tag{7}$$

Using Eq. (5) and Eq. (6), Eq. (4) can be rearranged as follows, giving the expression Eq. (8) for V_{cell}:

$$V_{cell} = IR_{int} + \frac{285840 - 163.2(273 + T)}{2F} \tag{8}$$

The total power consumed by the cell $P_{t,cell}$ (W) is expressed in Eq. (9):

$$P_{t,cell} = IV_{cell} \tag{9}$$

The hydrogen flow rate $v_{H,cell}$ (ml/min) is stated in Eq. (10) as a function of the consumed current I and the molar volume v_M (l) [43]:

$$v_{H,cell} = v_M(\mathrm{l})\left(\frac{10^3 \mathrm{ml}}{\mathrm{l}}\right)\left(\frac{60\ \mathrm{s}}{min}\right)\left(\frac{I\left(\frac{\mathrm{C.}}{\mathrm{s}}\right)}{2F\ (\mathrm{C.})}\right) = v_M(10^3)(60)\left(\frac{I}{2F}\right) \tag{10}$$

where v_M is obtained from Eq. (11) as a function of the working temperature T, the working pressure p (atm) and the ideal gas constant R (0.082 l atm K^{-1} mol^{-1}):

$$v_M(\mathrm{l}) = \frac{R(273+T)}{p} \tag{11}$$

Finally, the cell efficiency η_{cell} is given by Eq. (12) and is defined as the parameter that relates $P_{e,cell}$ and $P_{t,cell}$. Since both variables depend on I, the expression is reduced to the ratio between V_{int} and V_{cell}:

$$\eta_{cell} = \frac{P_{e,cell}}{P_{t,cell}} = \frac{IV_{int}}{IV_{cell}} = \frac{V_{int}}{V_{cell}} \tag{12}$$

3.2. Experimental process for the determination of the internal cell resistance

Among the equations presented in Section 3.1, R_{int} is the only cell parameter that cannot be measured or calculated directly. This parameter is crucial to determine the value of V_{cell}, so Eq. (8) has been rearranged to determine R_{int}, resulting in Eq. (13):

$$R_{int}(T,I) = \left[V_{cell}(T,I) - \left(\frac{285840 - 163.2(273+T)}{2F}\right)\right] \Big/ I \tag{13}$$

Eq. (13) expresses R_{int} as a function of T, I and V_{cell}. Thus, to obtain the values of the internal resistance over the complete range of T and I, it is required to know beforehand the value of V_{cell} at each operating point. To this end, an experimental process has been conducted to obtain an expression that defines the value of R_{int} within the operating range of the cell (T (°C) = {25,50} and I (A) = {0,8}).

Initially, the PEMEL has been subjected to various tests of constant current operation with temperature variation. In this way, the value of $V_{cell}(T,I)$ has been obtained for the whole temperature range in each of the operating currents. The data obtained during the test are gathered using the DAQ, visualised by the LABVIEW GUI and stored in an independent Excel spreadsheet for each of the tests. Subsequently, the data has been filtered and processed to calculate $R_{int}(T,I)$. As an example, Fig. 7a and b display the graphs $V_{cell}(T,I)$ and $R_{int}(T,I)$ respectively, obtained as a result of the test carried out at a current of 6 A for each of the cells.

To determine the expression of $R_{int}(T,I)$ from the experimental data obtained, the MATLAB Curve Fitting Toolbox [44] has been employed. This tool facilitates the fitting of curves and surfaces to the data provided by employing regression, interpolation and smoothing techniques. Concerning its operation, the toolbox requires input data to perform the fitting process. For this purpose, it is necessary that said data are previously loaded in the MATLAB Workspace. Therefore, as an initial step, for each cell, the experimental values of T,I and $R_{int}(T,I)$ are read from the Excel file in matrix format. Then, in the toolbox, the values of T, I and $R_{int}(T,I)$ are associated with the variables X,Y, and Z of the fitting expression, respectively. Finally, the desired type of fit is selected, optionally including a weight matrix that modifies the fitting configuration. As a result, the toolbox displays the surface generated from the fitting process, as well as the resulting mathematical expression, the values of the coefficients and a set of indices associated with the goodness of the fit (SEE, R-square, Adjusted R-square and RMSE). Fig. 8 depicts the interface of the Curve Fitting Toolbox for the case of the surface obtained from $R_{int}(T,I)$ of cell C1. This figure highlights the different areas that comprise the toolbox.

For this particular application, the "Custom Equation" fitting option has been employed, enabling the incorporation of a customisable expression. The expression integrated into the toolbox was achieved during the preliminary data filtration and initial analysis process within Excel, facilitated by the employment of the ThreeDify XLGrapher add-on [45]. This supplementary tool streamlines the three-dimensional representation of surfaces within Excel, utilising input data. Additionally, it facilitates a straightforward fitting process through a wide variety of equations. However, this add-on only represents the fitted surface according to the general equation selected, without indicating the mathematical expression that defines the surface or the values of its coefficients. Therefore, ThreeDify XLGrapher has been employed to determine the general equation used in the fitting process, while the MATLAB Curve Fitting toolbox has been used to obtain the complete particularised expression of $R_{int}(T,I)$ for each cell.

Fig. 9 expands the information displayed in the results window of the

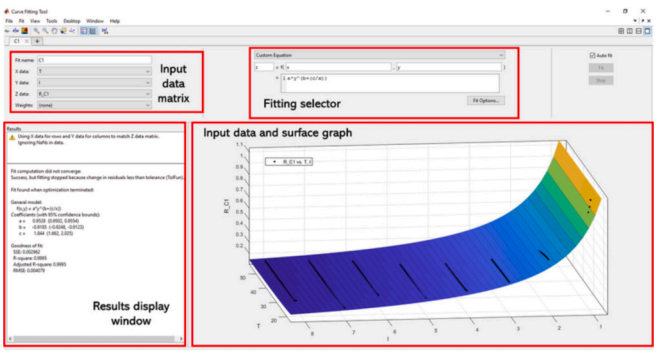

Fig. 8. MATLAB Curve Fitting Toolbox. Resulting surface for $R_{int}(T,I)$ of cell C1.

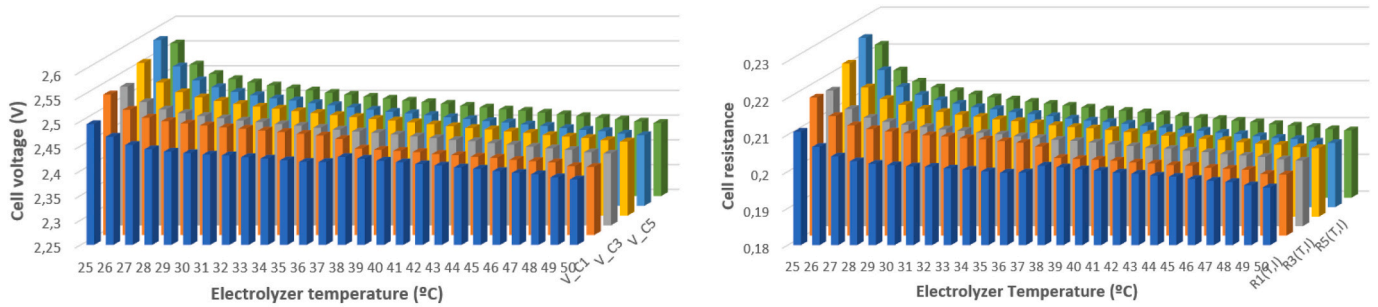

Fig. 7. Results obtained for each cell in the test at 6 A. (a) Values for $V_{cell}(T,I)$. (b) Values for $R_{int}(T,I)$.

General model:
f(x,y) = a*y^(b+(c/x))
Coefficients (with 95% confidence bounds):
a = 0.9528 (0.9502, 0.9554)
b = -0.9185 (-0.9248, -0.9123)
c = 1.844 (1.662, 2.025)

Fig. 9. Generated surface equation and coefficients of $R_{int}(T,I)$ for cell C1.

Curve Fitting toolbox, showing the expression used for the fit, called the "general model", as well as the values of the coefficients a, b and c.

For the remaining PEMEL cells, the process to determine $R_{int}(T,I)$ is homologous. This process is illustrated in Fig. 10, where a flowchart summarises the steps from obtaining experimental data through tests to determining the parameterised expression of internal resistance by means of the toolbox.

Once the process described in Fig. 10 has been completed, an equation is obtained for $R_{int}(T,I)$ of the cell expressed in Eq. (14). Table 2 lists the values of the coefficients particularised for each of the 6 cells that integrate the PEMEL.

$$R_{int}(T,I) = aI^{\left(b+\left(\frac{c}{T}\right)\right)} \tag{14}$$

Combining Eq. (14) and Eq. (8) results in an expression for V_{cell} dependent solely on T and I, as presented in Eq. (15). Based on this expression, the remaining parameters presented in Section 3.1 can be determined.

$$V_{cell}(T,I) = IaI^{\left(b+\left(\frac{c}{T}\right)\right)} + \frac{285840 - 163.2(273+T)}{2F} \tag{15}$$

3.3. PEMEL parameters

After obtaining the key parameters of the PEMEL cells by calculating

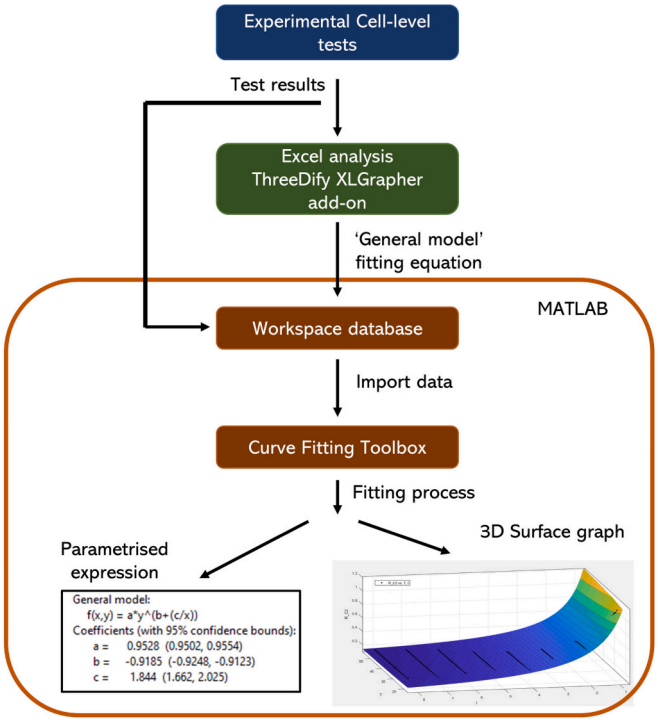

Fig. 10. $R_{int}(T,I)$ determination process for each cell.

Table 2
$R_{int}(T,I)$ coefficient values for each cell.

Cell	Coefficient a	Coefficient b	Coefficient c
C1	0.9528	−0.9185	1.844
C2	1.048	−0.9693	1.922
C3	1.09	−0.9756	1.384
C4	1.105	−0.9847	1.596
C5	1.103	−0.9981	2.035
C6	1.105	−0.9922	1.826

R_{int} and V_{cell}, the expressions that describe the behaviour of the PEMEL as a unit can be determined, under several considerations:

- The PEMEL stack presents a series structure, which implies that the current consumed I by the electrolyzer is the same as the current flowing through each of the cells.
- Due to the technical limitations of the developed installation, the temperature and pressure of the cells are considered to match those measured for the PEMEL as a unit.

Thus, the electrolyzer voltage V_{el} (V) expressed in Eq. (16) is obtained, where the index i refers to the cell number of the PEMEL.

$$V_{el} = \sum_{i=1}^{6} V_{cell}(T,I) = \sum_{i=1}^{6}\left(IaI^{\left(b_i+\left(\frac{c_i}{T}\right)\right)} + \frac{285840 - 163.2(273+T)}{2F}\right) \tag{16}$$

The effective power used by the PEMEL for the electrolysis process $P_{e,el}$ (W) is calculated by Eq. (17), where n_{cell} refers to the total number of cells that comprise the PEMEL:

$$P_{e,el} = In_{cell}V_{int} \tag{17}$$

The total power consumed by the PEMEL $P_{t,el}$ (W) is determined by Eq. (18):

$$P_{t,el} = IV_{el} \tag{18}$$

The total generated hydrogen flow rate $v_{H,el}$ (ml/min) is obtained using Eq. (19):

$$v_{H,el} = n_{cell}v_M(1)\left(\frac{10^3\,\text{ml}}{1}\right)\left(\frac{60\,\text{s}}{min}\right)\left(\frac{I\left(\frac{\text{C}}{\text{s}}\right)}{2F\ (\text{C})}\right) = n_{cell}v_M\left(10^3\right)(60)\left(\frac{I}{2F}\right) \tag{19}$$

Finally, the overall efficiency of the PEMEL η_{el} is expressed in Eq. (20) as the ratio between the useful voltage employed in the electrolysis and the total voltage of the electrolyzer:

$$\eta_{el} = \frac{P_{e,el}}{P_{t,el}} = \frac{In_{cell}V_{int}}{IV_{el}} = \frac{n_{cell}V_{int}}{V_{el}} \tag{20}$$

4. Results and discussion

After describing the expressions defining the individual cell and the PEMEL models, the suitability of DR is assessed by employing experimental data gathered from the PEMEL under its nominal operation.

First, the behaviour of the parametrised cell model for each PEMEL cell is tested. For this purpose, a comparison is made between the experimental (exp) and theoretical (teo) values of the variables V_{cell} and $R_{int}(T,I)$. The experimental values of V_{cell} reflect the directly measured voltage of each cell. The theoretical values of V_{cell} are determined from the model using Eq. (15) parametrised for each cell. Regarding $R_{int}(T,I)$, the experimental values are determined using Eq. (13), leveraging the experimental V_{cell} values. Meanwhile, the theoretical values are calculated from Eq. (14) obtained employing the MATLAB toolbox Curve Fitting and parameterised for each cell.

Fig. 11 presents a graphical comparison of these variables, depicting the set of R_{int}-T and V_{cell}-T curves for each individual cell.

As shown in the graphs presented in Fig. 11, the experimental and theoretical values of R_{int} and V_{cell} are similar, coinciding and overlapping in some cases, as in cells 5 and 6. Furthermore, the behaviour of both parameters is homologous with regard to temperature variations, presenting a downward trend with increases in the working temperature. This trend is reflected in a lower voltage for the same current consumed,

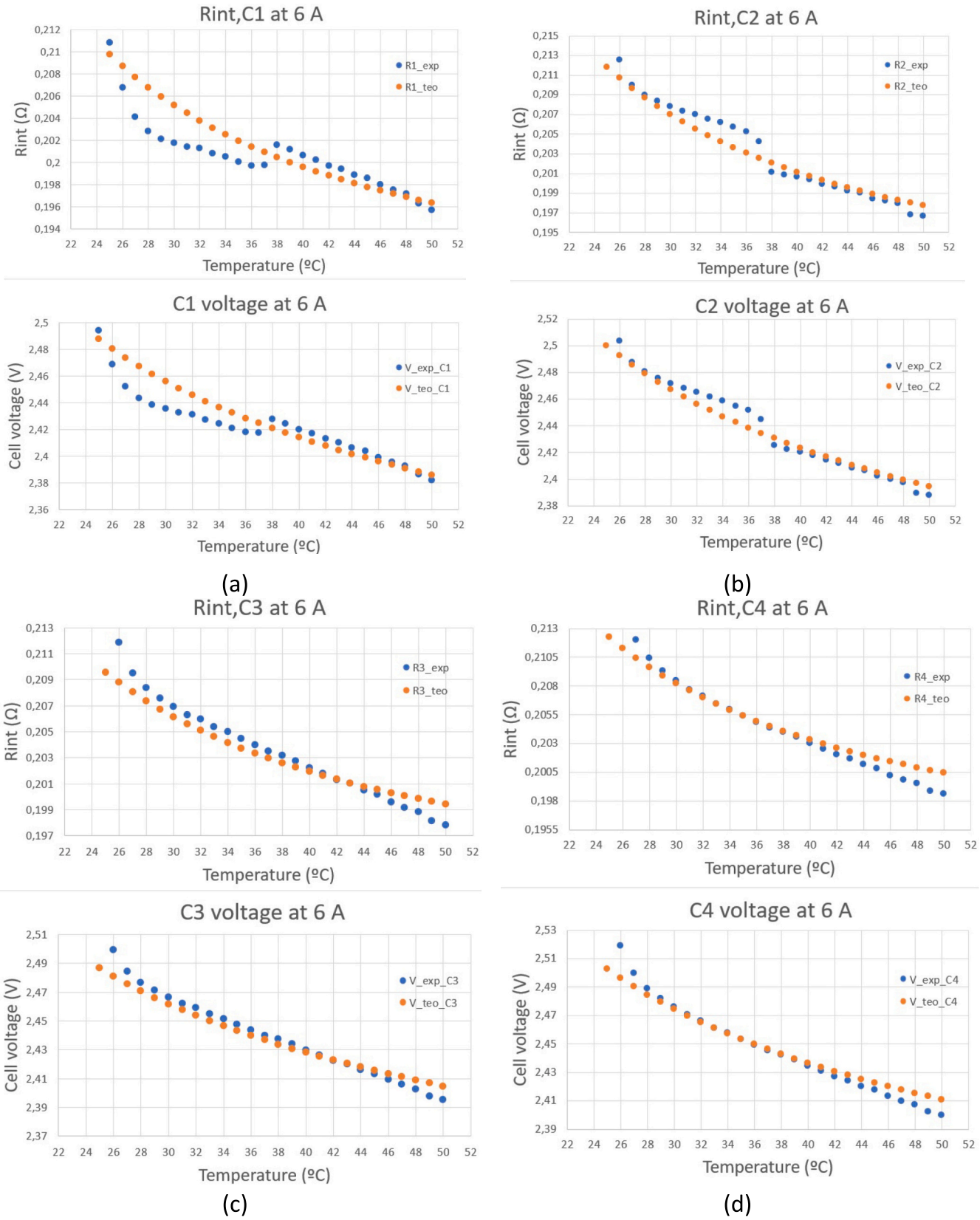

Fig. 11. R_{int}-T and V_{cell}-T curves obtained for each cell with a constant current of 6 A. (a) Cell 1. (b) Cell 2. (c) Cell 3. (d) Cell 4. (e) Cell 5. (f) Cell 6.

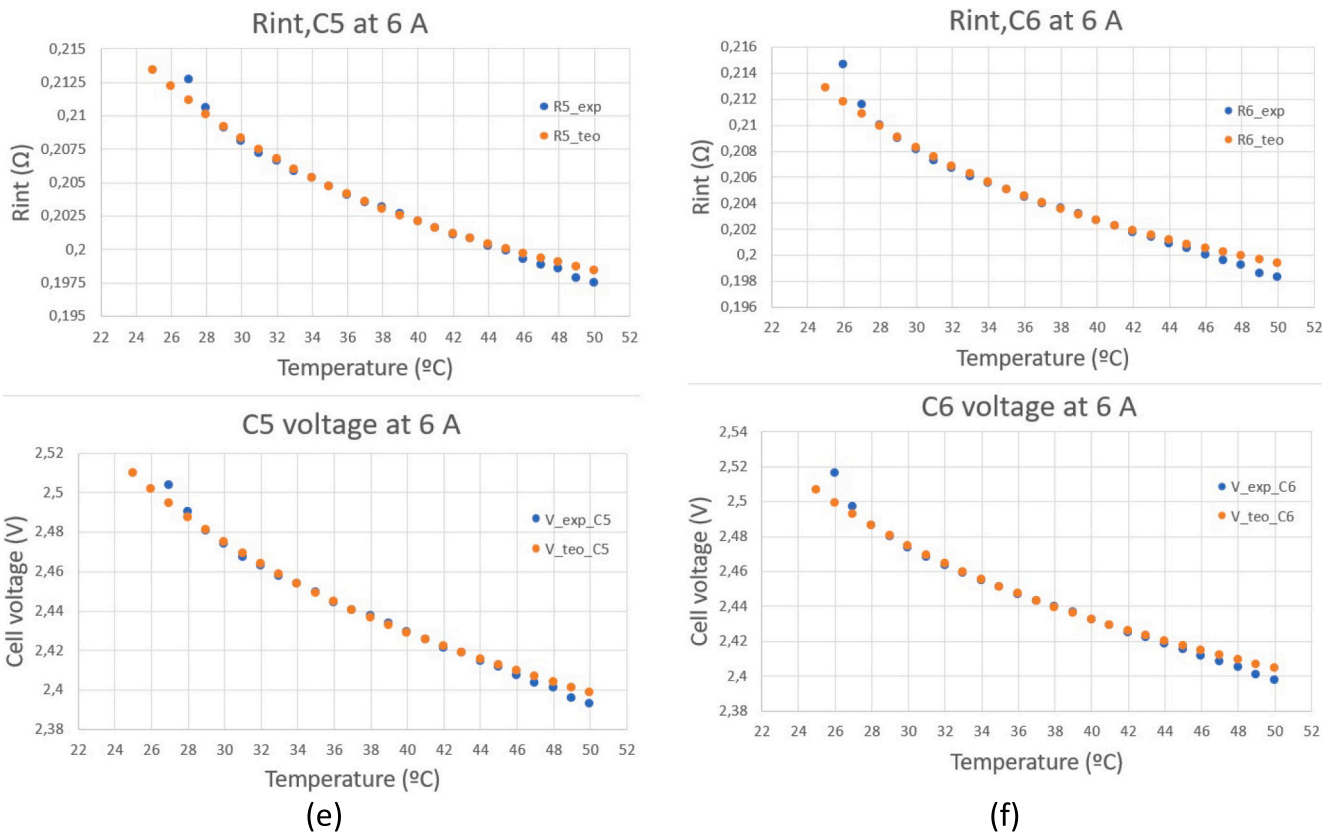

Fig. 11. (*continued*).

which results in a reduction of the total power consumed (Eq. 9) as well as an increase in the efficiency of the cell (Eq. 12).

To corroborate these results, a series of statistical metrics have been applied to the V_{cell} of each of the cells. Specifically, the Root Mean Square Error (RMSE), the Mean Absolute Error (MAE) and the Coefficient of Determination (R^2) have been applied.

The RMSE indicates the standard deviation of the residual values, which are a measure of the distance between the data points and the regression line. This metric allows quantifying the level of dispersion of the residual values and calculating the level of concentration of the data on the regression line. This metric is calculated by Eq. (21), where y_{exp} and y_{teo} refer to the values obtained experimentally and theoretically, respectively. Moreover, the parameter n indicates the sample size.

$$\mathrm{RMSE} = \sqrt{\frac{\sum_{i=1}^{n}\left(y_{exp,i} - y_{teo,i}\right)^2}{n}} \tag{21}$$

The MAE is a measure of the average magnitude of the absolute errors between experimental and theoretical measurements. This value is determined utilising Eq. (22).

$$\mathrm{MAE} = \frac{\sum_{i=1}^{n}\left|y_{exp,i} - y_{teo,i}\right|}{n} \tag{22}$$

R^2 illustrates the level of coincidence between the experimental data and those obtained in the theoretical model. Thus, R^2 presents a measure of the overall accuracy of the model. Such measure is evaluated by Eq. (23), where e refers to the difference between the experimental and theoretical values and $\overline{y_{exp}}$ indicates the average of the experimental values.

$$R^2 = 1 - \left(\frac{\sum e^2}{\sum\left(y_{exp} - \overline{y_{exp}}\right)^2}\right) \tag{23}$$

Table 3 reports the values obtained for these metrics for each cell voltage.

The values presented in Table 3 reflect a successful and accurate performance of the model at cell level. Regarding the RMSE, the calculated values are reduced and close to zero, indicating a high concentration between the experimental and theoretical values concerning the regression line. Furthermore, the MAE values reflect a narrow absolute error for each cell, which corroborates the correct static behaviour of the model. Finally, the R^2 obtained displays values close to the unit, which confirms the accuracy of the model.

After obtaining these results at cell level, the performance of the model was tested to determine the parameters of the PEMEL as a unit. For this purpose, the PEMEL is arranged under rated operating conditions in such a way that it covers the entire input current range in an upward direction. By obtaining the experimental data, the cell-level parameters have been calculated using the proposed model. Hereafter, the key parameters of the PEMEL have been determined theoretically. Once the experimental and theoretical PEMEL data have been obtained, the characteristic curves of the electrolyzer can be plotted and compared.

Table 3
Statistical metrics for each cell voltage derived from 6 A operation.

	RMSE	MAE	R^2
C1	0.01185519	0.00980082	0.75988013
C2	0.00945017	0.00666523	0.93704076
C3	0.01042611	0.00632603	0.89706081
C4	0.0128881	0.0064928	0.88255837
C5	0.01620467	0.00566716	0.86372224
C6	0.01105357	0.00426088	0.91337222

First, the V_{el}-I curve depicted in Fig. 12 illustrates the relationship between the input voltage and current of the PEMEL, representing the main curve that defines the behaviour of the electrolyzer. The values of V_{el_exp} have been obtained by direct measurement of the electrolyzer voltage, while V_{el_teo} has been calculated by means of Eq. (16).

This curve describes the operation of the PEMEL by means of two differentiated zones: a first zone located in the low current range (from 0 A to 0.5 A) and another one in the nominal current range (from 0.5 A to 8 A). In the first zone, an abrupt and sudden behaviour of the voltage is observed, represented by a variation from 0 V to 12–13 V. This phenomenon is due to the PEMEL requirement of a minimum operating current. When this condition is satisfied, the voltage varies spontaneously increasing to a first start voltage. As the input current is increased, the electrolyzer behaviour is described by the second zone. In the last region, the voltage traces a linear curve around 14–15 V, where the nominal value of the operating voltage is reached. The slope of this curve is dependent on the temperature and working pressure of the PEMEL, decreasing with increasing temperature and ascending with increasing pressure.

The $P_{t,el}$-I presented in Fig. 13 represents the relationship between the total power consumed and the input current. As indicated in Eq. (18), this relationship is linear, with a maximum value around 120 W for 8 A. P_{t,el_exp} and P_{t,el_teo} have been determined using Eq. (18), employing in the said equation, for each case, the values of V_{el_exp} and V_{el_teo}, respectively.

Fig. 14 depicts the $v_{H,el}$-I curve, which relates the total hydrogen flow rate generated and the current consumed. Similar to the $P_{t,el}$-I curve, it presents a linear geometry, reaching the nominal hydrogen production value (250 ml/min) for 7 A and a maximum value of around 300 ml/min at 8 A. The values of v_{H,el_exp} are obtained by measuring the hydrogen flow rate through the installed H_2 flow meter. v_{H,el_teo} is calculated by means of Eq. (19).

As a last characteristic curve, Fig. 15 shows the η_{el}-I curve, which illustrates the relationship between the overall efficiency of the PEMEL and the current consumed. This curve has an inverse geometry to the V_{el}-I curve, with the efficiency being higher in the low current range and decreasing as the current increases. This value stabilises for the nominal current range at around 0.5, which represents an overall efficiency of 50 % under nominal operating conditions. η_{el_exp} and η_{el_teo} have both been calculated by means of Eq. (20), employing the values of V_{el_exp} and V_{el_teo}, respectively.

The curves represented in Figs. 12 to 15 confirm a satisfactory performance of the described model, presenting values that are close and accurate to those measured experimentally for all the key parameters of the PEMEL. As in the case of the individual cells, this graphical comparison is supported by statistical metrics in order to numerically corroborate the suitability of the model presented in this research.

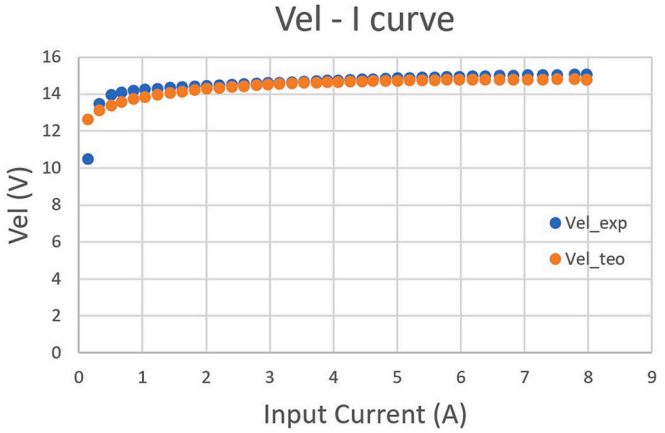

Fig. 12. PEMEL V_{el}-I curve.

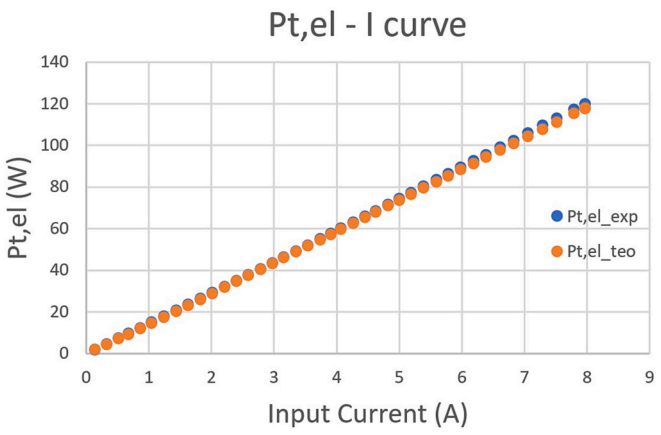

Fig. 13. PEMEL $P_{t,el}$-I curve.

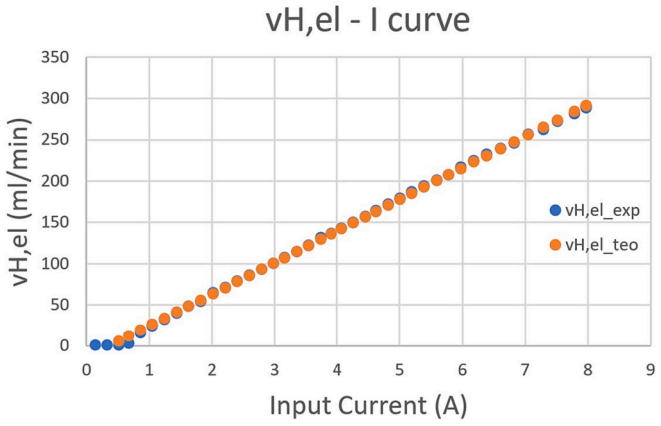

Fig. 14. PEMEL $v_{H,el}$-I curve.

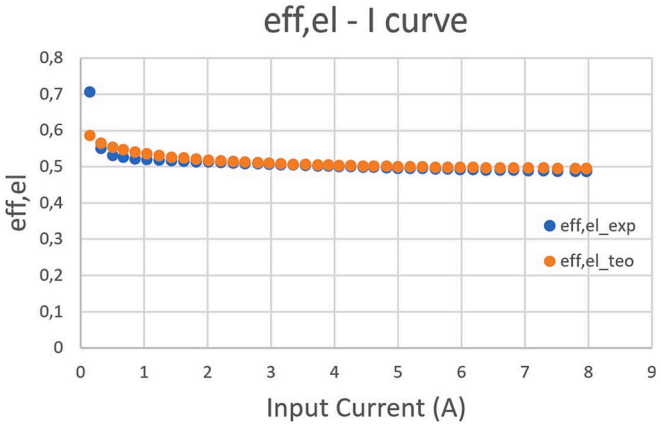

Fig. 15. PEMEL η_{el}-I curve.

Table 4
Statistical metrics for each key parameter of the PEMEL performance.

	RMSE	MAE	R^2
V_{el}	0.405435273	0.250501812	0.88535682
$P_{t,el}$	0.955620569	0.748756913	0.99927021
η_{el}	0.020408517	0.009754147	0.8363784
$V_{H,ell}$	0.977475729	0.768943431	0.99915947

Table 4 reports the values of the RMSE, MAE and R^2 metrics for the key parameters of the PEMEL.

Similar to the values shown in Table 3 for the case of individual cells, the metrics displayed for the PEMEL corroborate an optimal and accurate performance of the DR compared to the experimental data gathered. Regarding the RMSE, values lower than the unit are observed, denoting a high clustering between experimental and theoretical data, confirming a minimum dispersion.

Concerning MAE, the results obtained for the key variables denote a significantly reduced mean absolute error for the entire operating range of the PEMEL, which translates as an optimal and well-fitted operation of the DR. For instance, the MAE of $P_{t,el}$ is 0.75 W for an operating range with a maximum of 120 W. Within the nominal operating range (0.5 to 8 A), the total power consumed by the PEMEL remains considerably higher than the MAE of the DR, representing a negligible and acceptable deviation under the presented test conditions.

The R^2 metric exhibits a range of values between 0.83 and 0.99, close to the unit. These values corroborate the accuracy and suitability of the model applied in the DR for all the key variables of the PEMEL.

5. Conclusions

This paper has presented the design and validation of the DR of a PEMEL framed in a smart microgrid devoted to the generation of green hydrogen from water and photovoltaic energy for subsequent energy storage.

Regarding the equipment employed, the operating principle of the PEM cell and the main technical specification of the 6-cell PEMEL stack are described. Furthermore, the remaining ancillary equipment used in the installation for the proper operation of the PEMEL is outlined. A DAQ system has been implemented in order to gather, visualise and store experimental data by means of a PLC and a GUI designed in LabVIEW and communicated via OPC protocol.

For the design of the DR, an ECM-type model has been employed to describe the static behaviour of the individual cells that comprise the PEMEL. Moreover, this model facilitates the study of key variables such as voltage, total power consumed, hydrogen flow rate, and efficiency. This model is based on the determination of the internal resistance of the cell, which is a novelty in the literature, describing in detail all the stages required to obtain the designed model, and with it, the proposed DR.

The process conducted to obtain the model required several experimental tests and the utilisation of the MATLAB toolbox Curve Fitting to determine the expression of the particular internal resistance for each cell. A model for the PEMEL stack has been defined by obtaining the expressions of the key variables from the cell model.

The operation of the proposed DR has been tested for the cases of individual cells and the complete PEMEL, by means of a graphical and numerical comparison of the experimental and theoretical data. The results obtained verify the suitability and accuracy of the DR, corroborating the validity of the process described in the research.

From a practical standpoint, the experimental setup described in this work is comprised of commercial equipment, such as the PLC and various sensors utilised for measuring key variables. The nature of these devices streamlines the implementation and maintenance of the setup, without requiring equipment specifically manufactured for this application. Consequently, this approach achieves an adaptable and robust system that is easily reproducible and scalable.

In terms of technical requirements, the methodology employed for the development of the model relies mainly on two software environments: Excel and MATLAB. Both environments are widely known and used in the field of scientific research for their mathematical calculation capabilities, coinciding in their proprietary software nature. From a computational point of view, the data collected by the DAQ and the results obtained from the tests performed generate a moderate density of information. The magnitude of this dataset does not represent a processing problem (computational time, computational effort, etc.) for equipment such as current computers with modest technical specifications. Once the parameters have been determined using MATLAB curve fitting, the expressions to be coded for the calculations of the PEMEL variables are simple, facilitating their programming in automation and supervision equipment.

In relation to the context of the paper, the work presented is framed within the smart microgrids and renewable energies due to the equipment employed. Nevertheless, the results presented in this research are not limited to a single application within this framework. These results can be used in various contexts and applications thanks to the detailed description of the methodology developed.

Future work in relation to this line of research consists of comparing the proposed DR with other models in the literature, as well as applying the DR to the management of hydrogen generation systems by means of predictive strategies. In addition, the methodology employed in this paper could be applied to develop a DR of another PEMEL with different characteristics, such as number of cells, voltage and input current range, or flow rate of hydrogen generated. Finally, another line of future work involves the study of the dynamic behaviour of PEM cells and the experimental PEMEL.

CRediT authorship contribution statement

Francisco Javier Folgado: Conceptualization, Software, Investigation, Data curation, Writing- original draft, Review & editing. Isaías González: Methodology, Investigation, Writing- Preparation, Writing-review & editing. Antonio José Calderón: Conceptualization, Methodology, Validation, Investigation, Data curation, Writing – review & editing, Supervision.

Declaration of competing interest

The authors declare that they have no known competing financial interests or personal relationships that could have appeared to influence the work reported in this paper.

Data availability

The authors are unable or have chosen not to specify which data has been used.

Acknowledgements

Project co-financed by European Regional Development Funds FEDER and by the Junta de Extremadura (IB18041).

References

[1] K. Shinde, P.B. Mane, Review on high penetration of rooftop solar energy with secondary distribution networks using smart inverter, Energy Rep. 8 (2022) 5852–5860, https://doi.org/10.1016/j.egyr.2022.03.086.

[2] Y. Cao, E. Kamrani, S. Mirzaei, A. Khandakar, B. Vaferi, Electrical efficiency of the photovoltaic/thermal collectors cooled by nanofluids: machine learning simulation and optimization by evolutionary algorithm, Energy Rep. 8 (2022) 24–36, https://doi.org/10.1016/j.egyr.2021.11.252.

[3] K. Wang, W. Sun, W. Liu, X. Huo, R. Yin, J. Liu, et al., Mitigating interfacial and bulk defects via chlorine modulation for HTL-free all-inorganic $CsPbI_2Br$ carbon-based perovskite solar cells with efficiency over 14%, Chem. Eng. J. 445 (2022) 136781, https://doi.org/10.1016/j.cej.2022.136781.

[4] H. He, X. Wang, J. Chen, Y.-X. Wang, Regenerative fuel cell-battery-supercapacitor hybrid power system modeling and improved rule-based energy management for vehicle application, J. Energy Eng. 146 (2020) 04020060, https://doi.org/10.1061/(asce)ey.1943-7897.0000708.

[5] X. Yuan, J. Liu, C. Han, Y. Li, Y. Feng, Simultaneous nutrient-energy recovery from source-separated urine based on bioelectrically enhanced bipolar membrane-driven in-situ alkali production coupling with gas-permeable membrane system, Chem. Eng. J. 431 (2022) 134161, https://doi.org/10.1016/j.cej.2021.134161.

[6] I. González, A.J. Calderón, J.M. Andújar, Novel remote monitoring platform for RES-hydrogen based smart microgrid, Energ. Conver. Manage. 148 (2017) 489–505, https://doi.org/10.1016/j.enconman.2017.06.031.

[7] C. Li, J.B. Baek, The promise of hydrogen production from alkaline anion exchange membrane electrolyzers, Nano Energy 87 (2021) 106162, https://doi.org/10.1016/j.nanoen.2021.106162.
[8] K.W. Ahmed, M.J. Jang, M.G. Park, Z. Chen, M. Fowler, Effect of components and operating conditions on the performance of PEM electrolyzers: a review, Electrochem 3 (2022) 581–612, https://doi.org/10.3390/electrochem3040040.
[9] M. Ni, M.K.H. Leung, D.Y.C. Leung, Technological development of hydrogen production by solid oxide electrolyzer cell (SOEC), Int. J. Hydrogen Energy 33 (2008) 2337–2354, https://doi.org/10.1016/j.ijhydene.2008.02.048.
[10] A. Khataee, A. Shirole, P. Jannasch, A. Krüger, A. Cornell, Anion exchange membrane water electrolysis using AemionTM membranes and nickel electrodes, J. Mater. Chem. A 10 (2022) 16061–16070, https://doi.org/10.1039/d2ta03291k.
[11] M. Noussan, P.P. Raimondi, R. Scita, M. Hafner, The role of green and blue hydrogen in the energy transition—a technological and geopolitical perspective, Sustainability (Switzerland) 13 (2021) 1–26, https://doi.org/10.3390/su13010298.
[12] Y. Wang, Y. Pang, H. Xu, A. Martinez, K.S. Chen, PEM fuel cell and electrolysis cell technologies and hydrogen infrastructure development — a review, Energy Environ. Sci. 15 (2022) 2288–2328, https://doi.org/10.1039/d2ee00790h.
[13] D. Tang, G.L. Tan, G.W. Li, J.G. Liang, S.M. Ahmad, A. Bahadur, et al., State-of-the-art hydrogen generation techniques and storage methods: a critical review, J. Energy Storage 64 (2023) 107196, https://doi.org/10.1016/j.est.2023.107196.
[14] P.M. Falcone, M. Hiete, A. Sapio, Hydrogen economy and sustainable development goals: review and policy insights, Curr. Opin. Green Sustain. Chem. 31 (2021) 100506, https://doi.org/10.1016/j.cogsc.2021.100506.
[15] J.D. Hunt, A. Nascimento, N. Nascimento, L.W. Vieira, O.J. Romero, Possible pathways for oil and gas companies in a sustainable future: from the perspective of a hydrogen economy, Renew. Sustain. Energy Rev. 160 (2022) 112291, https://doi.org/10.1016/j.rser.2022.112291.
[16] D.E. Olivares, A. Mehrizi-Sani, A.H. Etemadi, C.A. Cañizares, R. Iravani, M. Kazerani, et al., Trends in microgrid control, IEEE Trans. Smart Grid 5 (2014) 1905–1919, https://doi.org/10.1109/TSG.2013.2295514.
[17] A. Hirsch, Y. Parag, J. Guerrero, Microgrids: a review of technologies, key drivers, and outstanding issues, Renew. Sustain. Energy Rev. 90 (2018) 402–411, https://doi.org/10.1016/j.rser.2018.03.040.
[18] T.M. Lawrence, M.C. Boudreau, L. Helsen, G. Henze, J. Mohammadpour, D. Noonan, et al., Ten questions concerning integrating smart buildings into the smart grid, Build. Environ. 108 (2016) 273–283, https://doi.org/10.1016/j.buildenv.2016.08.022.
[19] L.P. Van, K. Do Chi, T.N. Duc, Review of hydrogen technologies based microgrid: energy management systems, challenges and future recommendations, Int. J. Hydrogen Energy 48 (2023) 14127–14148, https://doi.org/10.1016/j.ijhydene.2022.12.345.
[20] O. Atlam, M. Kolhe, Equivalent electrical model for a proton exchange membrane (PEM) electrolyser, Energ. Conver. Manage. 52 (2011) 2952–2957, https://doi.org/10.1016/j.enconman.2011.04.007.
[21] Q. Feng, X.Z. Yuan, G. Liu, B. Wei, Z. Zhang, H. Li, et al., A review of proton exchange membrane water electrolysis on degradation mechanisms and mitigation strategies, J. Power Sources 366 (2017) 33–55, https://doi.org/10.1016/j.jpowsour.2017.09.006.
[22] A. Sánchez, Q. Zhang, M. Martín, P. Vega, Towards a new renewable power system using energy storage: an economic and social analysis, Energ. Conver. Manage. 252 (2022), https://doi.org/10.1016/j.enconman.2021.115056.
[23] A. Pujana, M. Esteras, E. Perea, E. Maqueda, P. Calvez, Hybrid-model-based digital twin of the drivetrain of a wind data generation, Energies 16 (2023), https://doi.org/10.3390/en16020861.
[24] A. Awasthi, K. Scott, S. Basu, Dynamic modeling and simulation of a proton exchange membrane electrolyzer for hydrogen production, Int. J. Hydrogen Energy 36 (2011) 14779–14786, https://doi.org/10.1016/j.ijhydene.2011.03.045.
[25] Á. Bárkányi, T. Chován, S. Németh, J. Abonyi, Modelling for digital twins—potential role of surrogate models, Processes 9 (2021), https://doi.org/10.3390/pr9030476.
[26] F.J. Folgado, I. González, A.J. Calderón, Simulation platform for the assessment of PEM electrolyzer models oriented to implement digital replicas, Energ. Conver. Manage. 267 (2022), https://doi.org/10.1016/j.enconman.2022.115917.
[27] D. Zhao, Q. He, J. Yu, M. Guo, J. Fu, X. Li, et al., A data-driven digital-twin model and control of high temperature proton exchange membrane electrolyzer cells, Int. J. Hydrogen Energy 47 (2022) 8687–8699, https://doi.org/10.1016/j.ijhydene.2021.12.233.
[28] T.M. Ismail, K. Ramzy, B.E. Elnaghi, M.N. Abelwhab, M.A. El-Salam, Using MATLAB to model and simulate a photovoltaic system to produce hydrogen, Energ. Conver. Manage. 185 (2019) 101–129, https://doi.org/10.1016/j.enconman.2019.01.108.
[29] Mohamed Albarghot, Mahmud Sasi, Luc Rolland, MATLAB/Simulink modeling and experimental results of a PEM electrolyzer powered by a solar panel, J. Energy Power Eng. 10 (2016), https://doi.org/10.17265/1934-8975/2016.12.009.
[30] D. Guilbert, G. Vitale, Dynamic emulation of a PEM electrolyzer by time constant based exponential model, Energies 12 (2019), https://doi.org/10.3390/en12040750.
[31] M. Espinosa-López, C. Darras, P. Poggi, R. Glises, P. Baucour, A. Rakotondrainibe, et al., Modelling and experimental validation of a 46 kW PEM high pressure water electrolyzer, Renew. Energy 119 (2018) 160–173, https://doi.org/10.1016/j.renene.2017.11.081.
[32] Á. Hernández-Gómez, V. Ramirez, D. Guilbert, B. Saldivar, Cell voltage static-dynamic modeling of a PEM electrolyzer based on adaptive parameters: development and experimental validation, Renew. Energy 163 (2021) 1508–1522, https://doi.org/10.1016/j.renene.2020.09.106.
[33] A.J. Calderón, I. González, M. Calderón, F. Segura, J.M. Andújar, A new, scalable and low cost multi-channel monitoring system for polymer electrolyte fuel cells, Sensors (Switzerland) 16 (2016), https://doi.org/10.3390/s16030349.
[34] I. González, A.J. Calderón, F.J. Folgado, IoT real time system for monitoring lithium-ion battery long-term operation in microgrids, J. Energy Storage 51 (2022) 104596, https://doi.org/10.1016/j.est.2022.104596.
[35] RTD PT100 datasheet (accessed on 14 March 2023) n.d. https://docs.rs-online.com/9186/0900766b815bb292.pdf.
[36] DC axial fan datasheet (accessed on 14 March 2023) n.d. https://docs.rs-online.com/6d6e/A700000007525942.pdf.
[37] Droking programmable DC/DC converter (accessed on 14 March 2023) n.d. https://www.droking.com/Power-Supply-Module-DC10V-75V-to-0-60V-12A-720W-Buck-Converter-Voltage-regulator-CNC-Control-Module-DC-12V-24V-36V-48V-Adapter.
[38] Bronkhorst mass flow meter datasheet (accessed on 14 May of 2023) n.d. https://www.bronkhorst.com/int/products/gas-flow/el-flow-select/f-111b/?pdf=true.
[39] Pressure transmiter Wika A-10 datasheet (accessed on 14 March 2023) n.d. https://shop.wika.com/media/Data-sheets/Pressure/Pressure-sensors/ds_pe8160_en_co.pdf.
[40] S7-1500 6ES7516-3AN00-0AB0 CPU datasheet (accessed on 14 March 2023) n.d. https://mall.industry.siemens.com/mall/en/ww/Catalog/DatasheetDownload?downloadUrl=teddatasheet%2F%3Fformat%3DPDF%26caller%3DMall%26mlfbs%3D6ES7516-3AN00-0AB0%26language%3Den.
[41] National Instruments (NI) LABVIEW main page (accessed on 14 March 2023) n.d. https://www.ni.com/en-gb/shop/labview.html.
[42] I. González, A.J. Calderón, J. Figueiredo, J.M.C. Sousa, A literature survey on open platform communications (OPC) applied to advanced industrial environments, Electronics (Switzerland) 8 (2019), https://doi.org/10.3390/electronics8050510.
[43] Fuel Cell Handbook, 6th ed., US National Energy Technology Laboratory, 2002. November. DOE/NETL-2002/1179.
[44] MATLAB curve fitting toolbox (accessed on 14 March 2023) n.d. https://uk.mathworks.com/products/curvefitting.html.
[45] ThreeDify XLGrapher (accessed on 12 August 2023) n.d. https://3dexcel.com/xlgrapher-3d-graphing-add-in-for-microsoft-excel/.